nature geoscience

SUPPLEMENTARY INFORMATION

https://doi.org/10.1038/s41561-019-0383-x

In the format provided by the authors and unedited.

Opposite tropical circulation trends in climate models and in reanalyses

Rei Chemke[1]* and Lorenzo M. Polvani[1,2]

[1]Department of Applied Physics and Applied Mathematics, Columbia University, New York, NY, USA. [2]Department of Earth and Environmental Sciences, and Lamont-Doherty Earth Observatory, Columbia University, Palisades, NY, USA. *e-mail: rc3101@columbia.edu

Opposite tropical circulation trends in climate models and in reanalyses

Rei Chemke[1] & Lorenzo M. Polvani[1,2]

[1]*Department of Applied Physics and Applied Mathematics, Columbia University, New York, NY 10027, USA*

[2]*Department of Earth and Environmental Sciences, and Lamont-Doherty Earth Observatory, Columbia University, Palisades, NY 10964, USA*

Table 1: List of the 40 CMIP5 models analyzed in this study.

	Model	Modeling Center
1	ACCESS1.0	CSIRO (Commonwealth Scientific and Industrial Research Organisation, Australia), and BOM (Bureau of Meteorology, Australia)
2	ACCESS1.3	CSIRO (Commonwealth Scientific and Industrial Research Organisation, Australia), and BOM (Bureau of Meteorology, Australia)
3	bcc-csm1-1	Beijing Climate Center, China Meteorological Administration
4	bcc-csm1-1-m	Beijing Climate Center, China Meteorological Administration
5	BNU-ESM	College of Global Change and Earth System Science, Beijing Normal University
6	CanESM2	Canadian Centre for Climate Modelling and Analysis
7	CCSM4	National Center for Atmospheric Research
8	CESM1-BGC	National Science Foundation, Department of Energy, National Center for Atmospheric Research
9	CESM1-CAM5-1-FV2	National Science Foundation, Department of Energy, National Center for Atmospheric Research
10	CESM1-CAM5	National Science Foundation, Department of Energy, National Center for Atmospheric Research
11	CMCC-CESM	Centro Euro-Mediterraneo per I Cambiamenti Climatici
12	CMCC-CM	Centro Euro-Mediterraneo per I Cambiamenti Climatici
13	CMCC-CMS	Centro Euro-Mediterraneo per I Cambiamenti Climatici
14	CNRM-CM5	Centre National de Recherches Meteorologiques / Centre Europeen de Recherche et Formation Avancees en Calcul Scientifique
15	CSIRO-Mk3-6-0	Commonwealth Scientific and Industrial Research Organisation in collaboration with the Queensland Climate Change Centre of Excellence
16	FGOALS-g2	LASG, Institute of Atmospheric Physics, Chinese Academy of Sciences; and CESS, Tsinghua University
17	FIO-ESM	The First Institute of Oceanography, SOA, China
18	GFDL-CM3	Geophysical Fluid Dynamics Laboratory
19	GFDL-ESM2G	Geophysical Fluid Dynamics Laboratory
20	GFDL-ESM2M	Geophysical Fluid Dynamics Laboratory
21	GISS-E2-H	NASA Goddard Institute for Space Studies
22	GISS-E2-H-CC	NASA Goddard Institute for Space Studies
23	GISS-E2-R	NASA Goddard Institute for Space Studies
24	GISS-E2-R-CC	NASA Goddard Institute for Space Studies
25	HadGEM2-AO	Met Office Hadley Centre (additional HadGEM2-ES realizations contributed by Instituto Nacional de Pesquisas Espaciais)
26	HadGEM2-CC	Met Office Hadley Centre (additional HadGEM2-ES realizations contributed by Instituto Nacional de Pesquisas Espaciais)

27	HadGEM2-ES	Met Office Hadley Centre (additional HadGEM2-ES realizations contributed by Instituto Nacional de Pesquisas Espaciais)
28	INMCM4	Institute for Numerical Mathematics
29	IPSL-CM5A-LR	Institut Pierre-Simon Laplace
30	IPSL-CM5A-LMR	Institut Pierre-Simon Laplace
31	IPSL-CM5B-LR	Institut Pierre-Simon Laplace
32	MIROC5	Atmosphere and Ocean Research Institute (The University of Tokyo), National Institute for Environmental Studies, and Japan Agency for Marine-Earth Science and Technology
33	MIROC-ESM	Japan Agency for Marine-Earth Science and Technology, Atmosphere and Ocean Research Institute (The University of Tokyo), and National Institute for Environmental Studies
34	MIROC-ESM-CHEM	Japan Agency for Marine-Earth Science and Technology, Atmosphere and Ocean Research Institute (The University of Tokyo), and National Institute for Environmental Studies
35	MPI-ESM-LR	Max Planck Institute for Meteorology (MPI-M)
36	MPI-ESM-MR	Max Planck Institute for Meteorology (MPI-M)
37	MRI-CGCM3	Meteorological Research Institute
38	MRI-ESM1	Meteorological Research Institute
39	NorESM1-M	Norwegian Climate Centre
40	NorESM1-ME	Norwegian Climate Centre

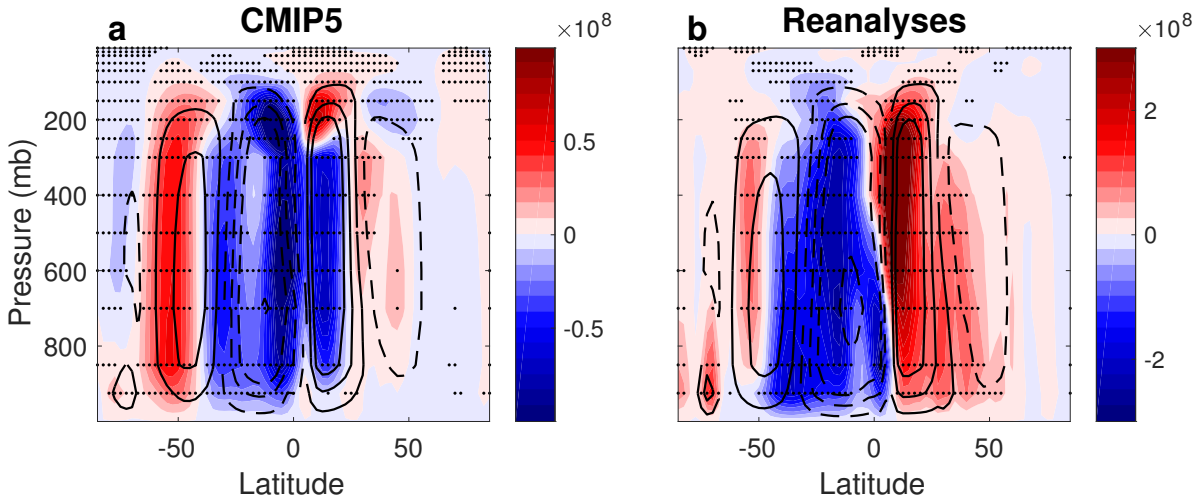

Fig. 1. **39-year (1979-2017) trends** ($\mathrm{kgs}^{-1}\mathrm{yr}^{-1}$) **of meridional mass streamfunction** (Ψ)**. a**, CMIP5 multi-model mean. **b,** Multi-reanalyses mean. In both panels colors show trends, and black contours show the climatology (1979-1989) streamfunction, where solid (dashed) contours represent clockwise circulation (counterclockwise). Contours show values of $\pm[0.1\,0.3\,0.5\,1\,1.6]\cdot 10^{11}$. The black dots show where the trends are statistically significant at the 95% confidence level.

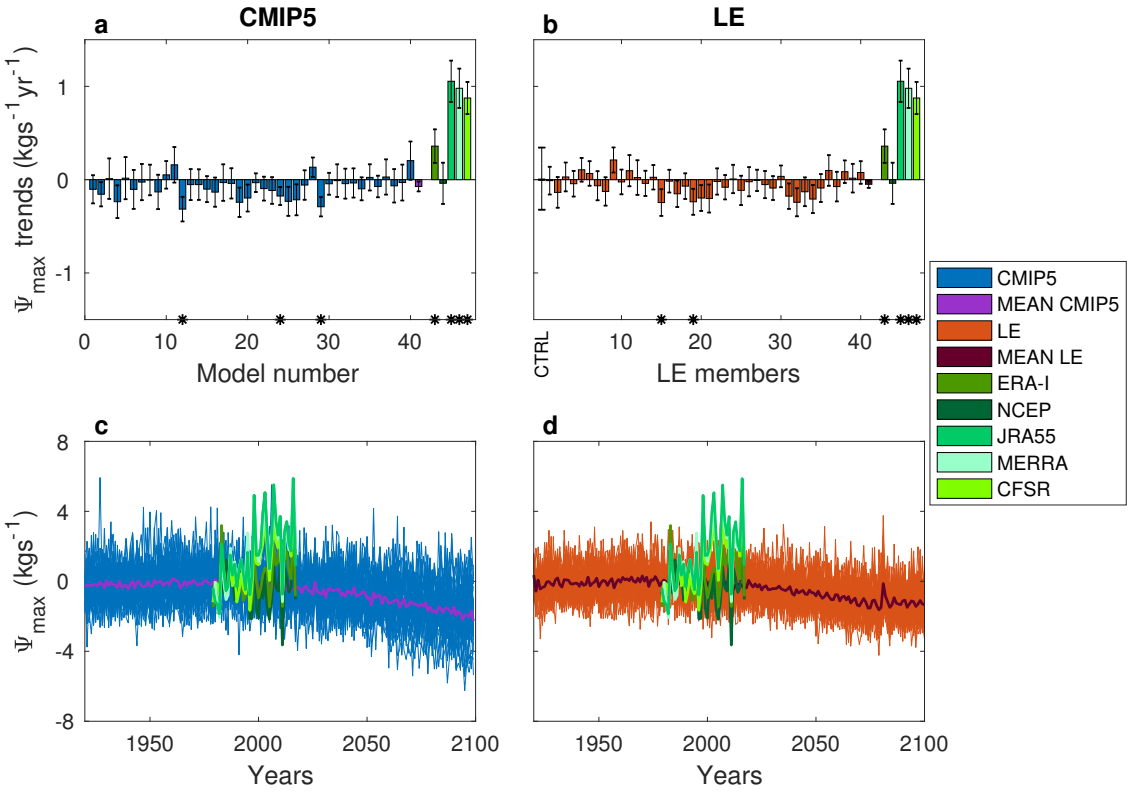

Fig. 2. **39-year (1979-2017) trends** (10^9 kgs^{-1}yr^{-1}) **and time series** (10^{10} kgs^{-1}) **of Northern Hemisphere DJF Hadley cell strength** ($\Psi_{\max}$)**. a**, Trends in CMIP5 models (blue bars) and their multi-model mean (purple bar). **b,** Trends in LE members (red bars) and their mean (maroon bar). The leftmost bar show the internal variability of 39-year trends calculated from the preindustrial control CESM run. **c,** Time series of Hadley cell strength in CMIP5 models (blue bars) and their multi-model mean (purple bar). **d,** Time series of Hadley cell strength in LE models (red bars) and their mean (maroon bar). The time series are relative to the 1979-1989 period. In all panels green symbols represent results from reanalyses. The trends from MERRA2 are available since 1980. The asterisks in **a** and **b** show that the trends are statistically significant (p-values lower than 0.1).

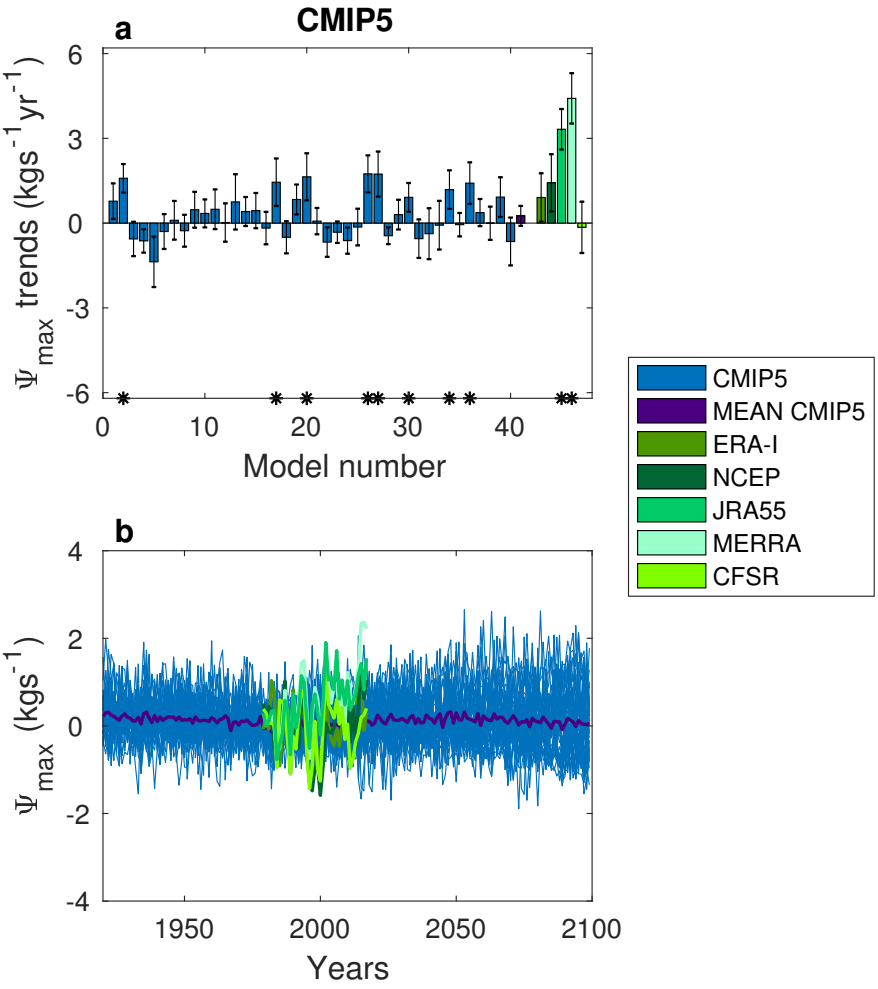

Fig. 3. **39-year (1979-2017) trends** (10^8 kgs^{-1}yr^{-1}) **and time series** (10^{10} kgs^{-1}) **of Southern Hemisphere Hadley cell strength** ($\Psi_{\max}$)**. a**, Trends in CMIP5 models (blue bars) and their multi-model mean (purple bar). **b,** Time series of HC strength in CMIP5 models (blue bars) and their multi-model mean (purple bar). In both panels green symbols represent results from reanalyses. The trends from MERRA2 are available since 1980. The asterisks in **a** show that the trends are statistically significant (p-values lower than 0.1), and the error bars show the standard error of linear regression coefficient.

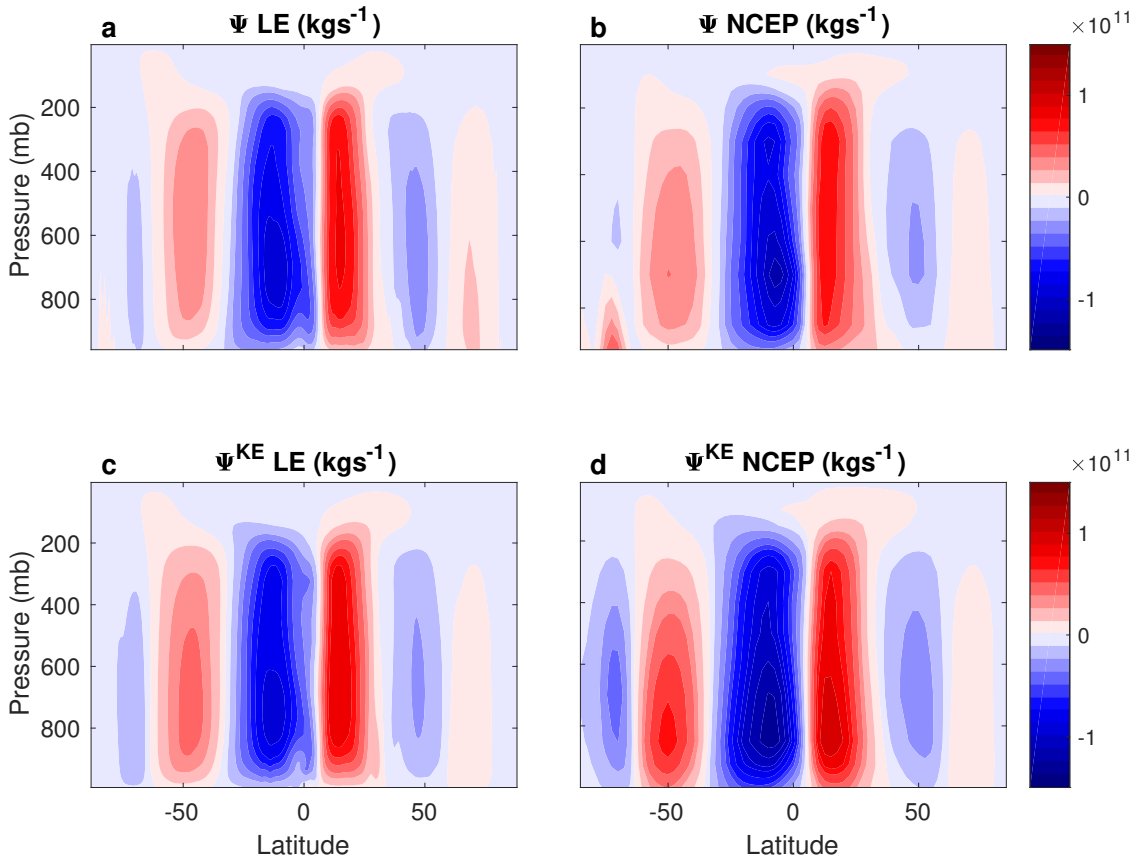

Fig. 4. **The solution for the streamfunction based on the KE equation.** The 1979 streamfunction computed from Methods Eq. 1, Ψ (upper row), and Methods Eq. 2, Ψ^{KE} (bottom row), in **a** and **c,** member #10 of the LE and **b** and **d,** NCEP reanalysis.

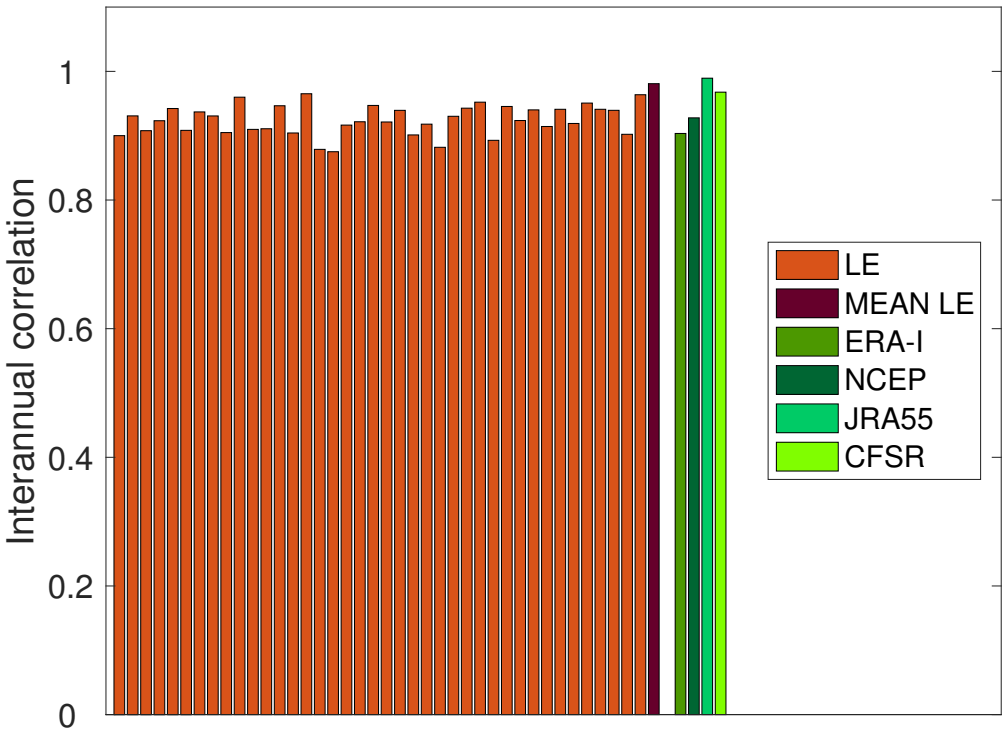

Fig. 5. **39-year (1979-2017) interannual correlation between the Hadley cell strength ($\Psi_{\max}$, Methods Eq. 1) and the Hadley cell strength based on the solution of the KE equation ($\Psi^{\mathrm{KE}}_{\max}$, Methods Eq. 2).** Red bars represent the LE (mean LE in maroon) and green bars represent reanalyses.

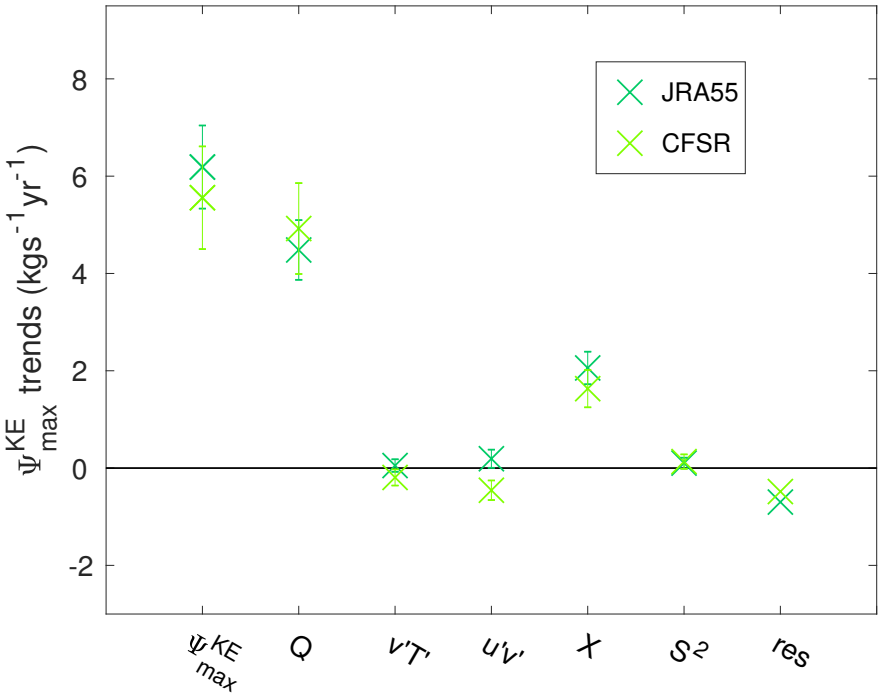

Fig. 6. 32-year (1979-2010) trends (10^8 $\mathrm{kgs^{-1}yr^{-1}}$) **of Northern Hemisphere Hadley cell strength in reanalyses calculated from the KE equation** ($\Psi^{\mathrm{KE}}_{\mathrm{max}}$) **using model-produced diabatic heating.** The relative contributions to the trends of the solution of the KE equation ($\Psi^{\mathrm{KE}}_{\mathrm{max}}$, Methods Eq. 4) from: model-produced diabatic heating (Q), eddy heat fluxes ($\mathrm{v'T'}$), eddy momentum fluxes ($\mathrm{u'v'}$), zonal friction (X), static stability (S^2) and the residual. Error bars show the standard error of linear regression coefficient. As shown in Fig. 2b in the manuscript using the diabatic heating from the thermodynamic equation, also here, using the model-produced diabatic heating, the component that mostly contributes to the strengthening of the circulation in reanalyses, and thus to the discrepancy between models and reanalyses, is the diabatic heating term.

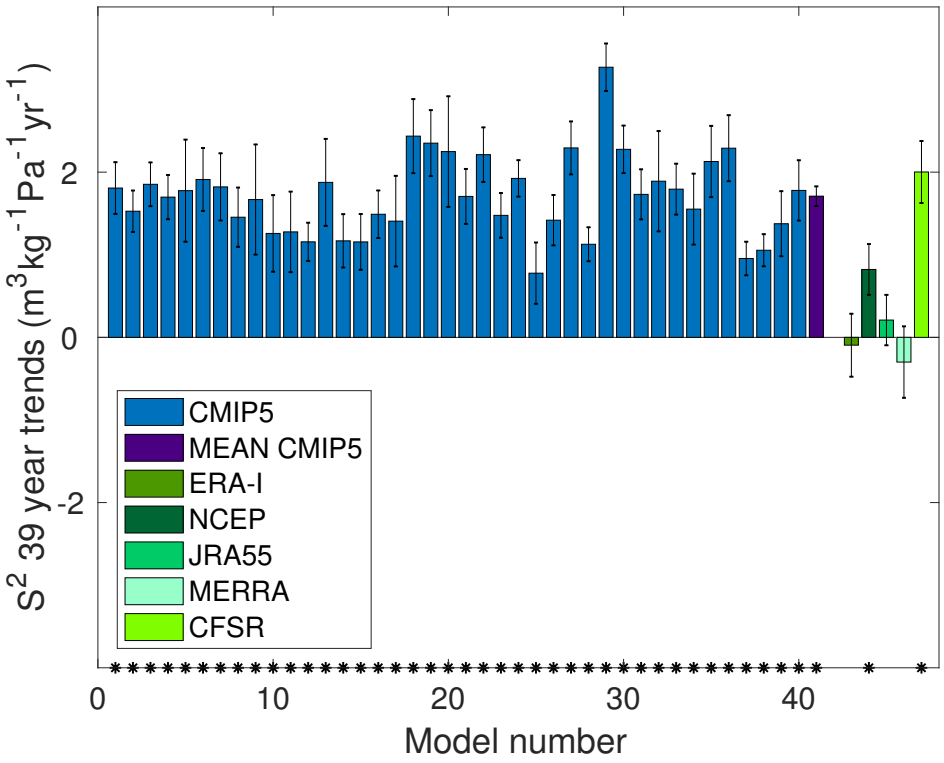

Fig. 7. 39-year (1979-2017) trends (10^{-9} $\mathrm{m^3 kg^{-1} Pa^{-1} yr^{-1}}$) **of mid-troposphere (500-850 mb) static stability** (S^2) **over the ascending branch of the Northern Hemisphere Hadley cell.** The ascending branch is defined between the Inter Tropical Convergence Zone (defined where the Ψ changes sign at $500\,\mathrm{mb}$between the Southern and Northern Hemisphere Hadley cells) and the latitude of Ψ_{max}. Blue, purple and green bars show the trends in CMIP5 models, their multi-model mean, and reanalyses, respectively. The asterisks show that the trends are statistically significant (p-values lower than 0.1), and the error bars show the standard error of linear regression coefficient.

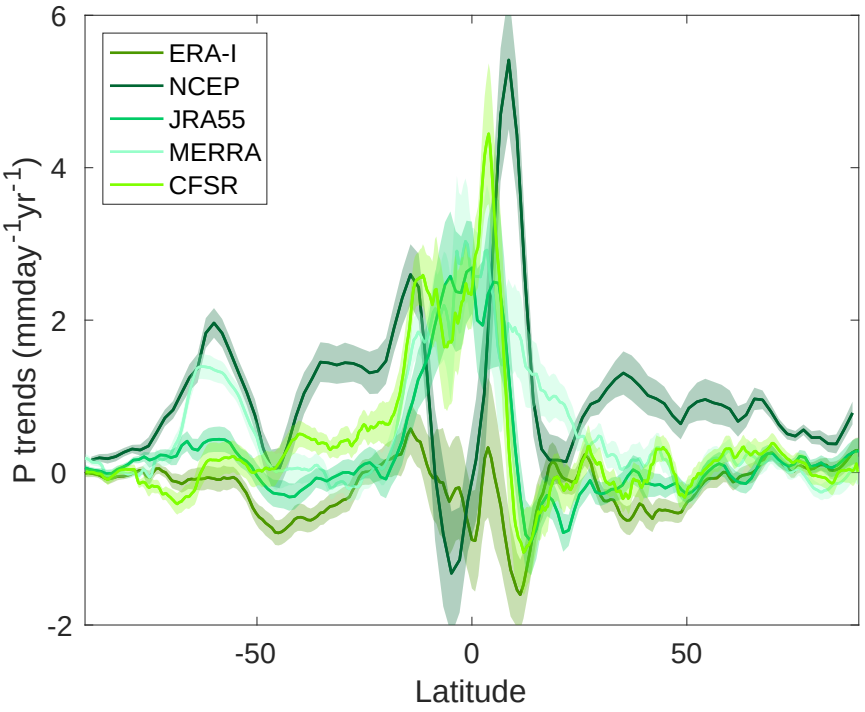

Fig. 8. 32-year (1979-2010) precipitation (10^{-2} mmday^{-1}yr^{-1}) trends in reanalyses as a function of latitude.

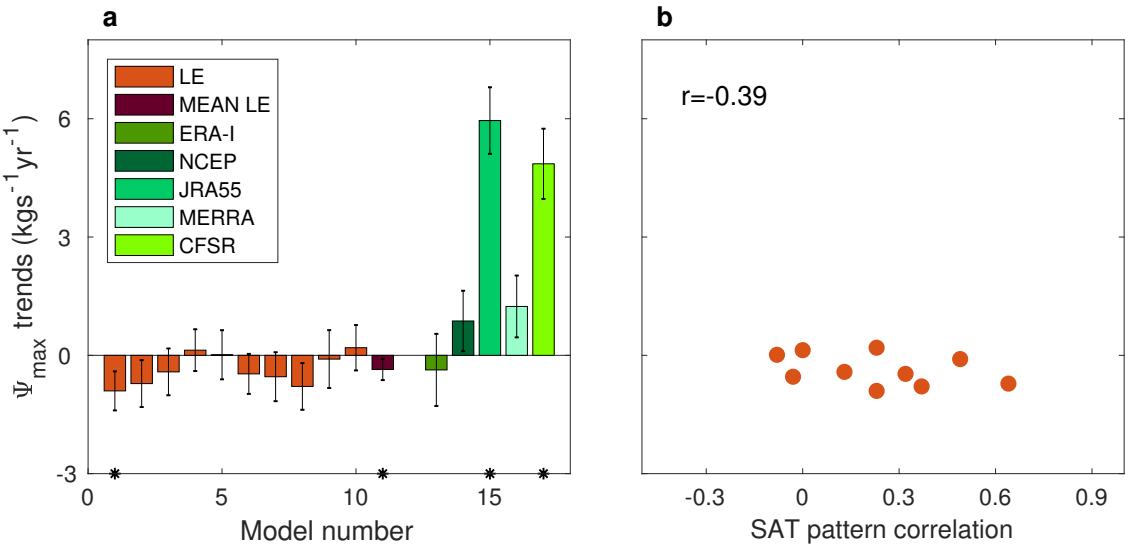

Fig. 9. 35-year (1979-2013) trends (10^8 kgs^{-1}yr^{-1}) **of Northern Hemisphere Hadley cell strength** ($\Psi_{\max}$) **in 'Pacemaker' runs. a**, $\Psi_{\max}$ trends in all members and reanalyses. **b**, $\Psi_{\max}$ trends in the Pacemaker runs as a function of the pattern correlation of surface air temperature (SAT) in the Pacemaker runs and the observed SAT (taken from 34). Red symbols show trends in LE members (mean in maroon), and green bars in reanalyses. The asterisks show that the trends are statistically significant (p-values lower than 0.1), and the error bars show the standard error of linear regression coefficient. The trends from MERRA2 are available since 1980.